Fluctuations and correlations of net baryon number, electric charge, and strangeness: A comparison of lattice QCD results with the hadron resonance gas model

A. Bazavov, Tanmoy Bhattacharya, C. E. DeTar, H.-T. Ding, Steven Gottlieb, Rajan Gupta, P. Hegde, Urs M. Heller, F. Karsch, E. Laermann, L. Levkova, Swagato Mukherjee, P. Petreczky, Christian Schmidt, R. A. Soltz, W. Soeldner, R. Sugar, and Pavlos M. Vranas
(HotQCD Collaboration)

Fluctuations and Correlations of net baryon number, electric charge, and strangeness: A comparison of lattice QCD results with the hadron resonance gas model

A. Bazavov[a], Tanmoy Bhattacharya[b], C. E. DeTar[c], H.-T. Ding[a], Steven Gottlieb[d], Rajan Gupta[b], P. Hegde[a], Urs M. Heller[e], F. Karsch[a,f], E. Laermann[f], L. Levkova[c], Swagato Mukherjee[a], P. Petreczky[a], Christian Schmidt[f], R.A. Soltz[g], W. Soeldner[h], R. Sugar[i], and Pavlos M. Vranas[g]

(HotQCD Collaboration)

[a] *Physics Department, Brookhaven National Laboratory, Upton, NY 11973, USA*
[b] *Theoretical Division, Los Alamos National Laboratory, Los Alamos, NM 87545, USA*
[c] *Department of Physics and Astronomy, University of Utah, Salt Lake City, UT 84112, USA*
[d] *Physics Department, Indiana University, Bloomington, IN 47405, USA*
[e] *American Physical Society, One Research Road, Ridge, NY 11961, USA*
[f] *Fakultät für Physik, Universität Bielefeld, D-33615 Bielefeld, Germany*
[g] *Physics Division, Lawrence Livermore National Laboratory, Livermore CA 94550, USA*
[h] *Institut für Theoretische Physik, Universität Regensburg, D-93040 Regensburg, Germany*
[i] *Physics Department, University of California, Santa Barbara, CA 93106, USA*

We calculate the quadratic fluctuations of net baryon number, electric charge and strangeness as well as correlations among these conserved charges in (2+1)-flavor lattice QCD at zero chemical potential. Results are obtained using calculations with tree level improved gauge and the highly improved staggered quark (HISQ) actions with almost physical light and strange quark masses at three different values of the lattice cut-off. Our choice of parameters corresponds to a value of 160 MeV for the lightest pseudo scalar Goldstone mass and a physical value of the kaon mass. The three diagonal charge susceptibilities and the correlations among conserved charges have been extrapolated to the continuum limit in the temperature interval 150 MeV $\leq T \leq$ 250 MeV. We compare our results with the hadron resonance gas (HRG) model calculations and find agreement with HRG model results only for temperatures $T \lesssim$ 150 MeV. We observe significant deviations in the temperature range 160 MeV $\lesssim T \lesssim$ 170 MeV and qualitative differences in the behavior of the three conserved charge sectors. At $T \simeq$ 160 MeV quadratic net baryon number fluctuations in QCD agree with HRG model calculations while, the net electric charge fluctuations in QCD are about 10% smaller and net strangeness fluctuations are about 20% larger. These findings are relevant to the discussion of freeze-out conditions in relativistic heavy ion collisions.

I. INTRODUCTION

The low energy runs currently being performed at the Relativistic Heavy Ion Collider (RHIC) [1] aim at an exploration of the QCD phase diagram at non-zero temperature (T) and baryon chemical potential (μ_B) through the measurement of fluctuations of conserved charges, *e.g.*, net baryon number, electric charge and strangeness. For the former, first results have been published by the STAR collaboration [2] and preliminary results on the latter two have been presented at conferences. A central goal of these experiments is to search for the existence of the QCD critical point, a second order phase transition point, that has been postulated to exist at non-vanishing baryon chemical potential in the T-μ_B phase diagram of QCD [3, 4]. Fluctuations in conserved charges can probe this critical point, the endpoint of a line of first order phase transitions that extends to large baryon chemical potential at non-zero quark masses. More generally, the study of fluctuations at any value of the baryon chemical potential probe thermal conditions in a medium and provide information on the critical behavior of QCD [5].

At zero baryon chemical potential, already, the analysis of fluctuations of conserved charges and their higher order cumulants provides important information about the relation between the QCD chiral phase transition at vanishing light quark masses, the cross-over temperature at physical quark masses and the freeze-out conditions observed in heavy ion experiments [5–7]. Thus, calculations of conserved charge fluctuations at $\mu_B = 0$ will provide unique information on freeze-out conditions at the LHC where the baryon chemical potential is small, $\mu_B/T \approx 0.05$. The quadratic fluctuations of the net baryon number characterize the width of the probability distribution which has been measured at RHIC [2] and has recently been analyzed in the framework of the hadron resonance gas (HRG) model [8]. Although the HRG model provides a rather satisfactory description of global hadron yields at chemical freeze-out [9], its ability to describe detailed properties of strongly interacting matter such as fluctuations of conserved charges and, in particular, their higher order cumulants is not obvious. The foundation for the HRG model is given by the Dashen, Ma, Bernstein theorem [12], which shows that the partition function of strongly interacting matter can be described by a gas of free resonances, if the system is sufficiently dilute and the resonance production is the dominant part of the interaction among hadrons [13, 14]. At very low temperature and high baryon number density, where nonresonant nucleon-nucleon interactions become important, as well as at high temperature where strongly interacting matter undergoes a transition to the quark-gluon plasma regime and partonic degrees of freedom become dominant, the HRG model is expected to be a poor approximation to the thermodynamics of strongly interacting matter. To what extent the HRG model provides a good description of strongly interacting matter needs to be explored in detail by comparing model calculations with first principal (lattice) QCD calculations. The latter provides the complete description of QCD thermodynamics at all values of the temperature and ultimately should set the standard for the interpretation of experimental results on strong interaction thermodynamics. Unfortunately, this is, at present, not fully possible. For instance, the only satisfactory way to specify the thermal conditions in a heavy ion experiment at the time of hadronization is through the comparison of experimental data with HRG model calculations [15]. It has recently been pointed out that in the future this may be overcome by comparing experimental data on conserved charge fluctuations directly with lattice QCD calculations [5]. Also in order to establish such an approach more firmly it is important to understand and quantify to what extent lattice QCD calculations and HRG model calculations agree and in which temperature regime the latter provides a reasonable approximation to strong interaction thermodynamics.

Indeed, some deviations in ratios of higher order cumulants of baryon number fluctuations, calculated within the HRG model, from experimental results for cumulants of net proton fluctuations have been observed [8]. Whether these deviations can be accounted for within QCD or are of more technical origin related to the restricted phase space in which experimental observations have been performed is an open question. In any case, a more detailed analysis of the thermal conditions achieved in heavy ion experiments is important. Lattice QCD calculations of fluctuations of conserved charges in equilibrium thermodynamics provide a base line for such discussions. Studies of fluctuations and higher order cumulants [16] may reveal differences between HRG model calculations and QCD thermodynamics that will appear close to criticality in the QCD phase diagram.

In this paper we will use the HRG model in its simplest version, i.e. as a sum of non-interacting, point-like particles. This is known to provide an accurate description of a dilute, strongly interacting hadron gas [13]. The need for taking into account residual interactions, for instance through the introduction of an intrinsic size of the hadrons [10] has been discussed. It has also been noted that the inclusion of higher mass resonances and an improvement in the strangeness sector of the HRG model may be needed to adequately describe pronounced features of hadron production such as the enhancement in the K/π ratio [11]. The advantage of the simplest version, however, is that the HRG model in this form is parameter free, while any improvement on this model will introduce further parameters without bringing us closer to the actual underlying theory, QCD, in a controlled way.

Quadratic fluctuations of conserved charges are closely related to quark number susceptibilities [17]. Fluctuations of net baryon number, electric charge and strangeness, as well as correlations among them, have been analyzed in previous lattice QCD calculations [18–21] and have also been used to characterize properties of the relevant thermodynamic degrees of freedom at low as well as high temperature [16, 22, 23]. The generic forms of their temperature dependence

and their scaling properties are understood in terms of universal properties of the QCD partition function and its derivatives in the vicinity of the QCD chiral phase transition [7, 20]. To make use of this knowledge in a quantitative comparison with experimental results, lattice QCD calculations close to the continuum are needed.

In this paper we present an analysis of fluctuations in, and correlations among, conserved charges using numerical calculations in (2+1)-flavor QCD at three values of the lattice cut-off [1]. For these calculations we exploit an $\mathcal{O}(a^2)$ improved action consisting of a tree-level improved gauge action combined with the highly improved staggered fermion action (HISQ/tree) [26, 27]. We discuss the cut-off dependence of our results in different temperature intervals and consider two different zero-temperature observables for the determination of the temperature scale used for extrapolations to the continuum limit. This allows us to quantify systematic errors in our calculation. In an appendix, we discuss the relation between temperature scales deduced from different zero-temperature observables and the propagation of their cut-off dependence into the cut-off dependence of thermodynamic observables.

II.   FLUCTUATIONS OF CONSERVED CHARGES FROM LATTICE QCD; THE HADRON RESONANCE GAS AND THE IDEAL GAS LIMIT

To calculate fluctuations of baryon number (B), electric charge (Q) and strangeness (S) from (lattice) QCD we start from the QCD partition function with non-zero light (μ_u, μ_d) and strange quark (μ_s) chemical potentials. The quark chemical potentials can be expressed in terms of chemical potentials for baryon number (μ_B), strangeness (μ_S) and electric charge (μ_Q),

$$\mu_u = \frac{1}{3}\mu_B + \frac{2}{3}\mu_Q \ ,$$
$$\mu_d = \frac{1}{3}\mu_B - \frac{1}{3}\mu_Q \ ,$$
$$\mu_s = \frac{1}{3}\mu_B - \frac{1}{3}\mu_Q - \mu_S \ . \tag{1}$$

The starting point of the analysis is the pressure p given by the logarithm of the QCD partition function,

$$\frac{p}{T^4} \equiv \frac{1}{VT^3} \ln Z(V, T, \mu_B, \mu_S, \mu_Q) \ . \tag{2}$$

Fluctuations of the conserved charges and their correlations in a thermalized medium are then obtained from its derivatives evaluated at $\vec{\mu} = (\mu_B, \mu_Q, \mu_S) = 0$,

$$\hat{\chi}_2^X \equiv \frac{\chi_2^X}{T^2} = \left. \frac{\partial^2 p/T^4}{\partial \hat{\mu}_X^2} \right|_{\vec{\mu}=0} \ , \tag{3}$$

$$\hat{\chi}_{11}^{XY} \equiv \frac{\chi_{11}^{XY}}{T^2} = \left. \frac{\partial^2 p/T^4}{\partial \hat{\mu}_X \partial \hat{\mu}_Y} \right|_{\vec{\mu}=0} \ , \tag{4}$$

with $\hat{\mu}_X \equiv \mu_X/T$ and $X, Y = B, Q, S$. Explicit expressions for the calculation of these susceptibilities in terms of generalized light and strange quark number susceptibilities are given in [20].

As all these derivatives are evaluated at $\vec{\mu} = 0$, the expectation values of all net charge numbers $\delta N_X \equiv N_X - N_{\bar{X}}$, with N_X $(N_{\bar{X}})$, denoting the number of particles (anti-particles), vanish, $i.e.$, $\langle \delta N_X \rangle = 0$. The susceptibilities, $i.e.$, the quadratic fluctuations of the charges, are then given by

$$\hat{\chi}_2^X = \langle (\delta N_X)^2 \rangle / VT^3 \ . \tag{5}$$

A.   The hadron resonance gas

We will compare results for fluctuations and correlations defined by Eqs. (3) and (4) with hadron resonance gas model calculations. The partition function of the HRG model can be split into mesonic and baryonic contributions,

$$\frac{p^{HRG}}{T^4} = \frac{1}{VT^3} \sum_{i \in \ mesons} \ln \mathcal{Z}_{M_i}^M(T, V, \mu_Q, \mu_S)$$

	B	Q	S
B	1/3	0	-1/3
Q	0	2/3	1/3
S	-1/3	1/3	1

TABLE I. Ideal gas values for off-diagonal, $\hat{\chi}_{11}^{XY} \equiv \chi_{11}^{XY}/T^2$, and diagonal susceptibilities, $\hat{\chi}_2^X \equiv \hat{\chi}_{11}^{XX}$. Here X, $Y = B$, Q, S.

$$+\frac{1}{VT^3} \sum_{i \in \, baryons} \ln \mathcal{Z}_{M_i}^B(T, V, \mu_B, \mu_Q, \mu_S) \,, \tag{6}$$

where the partition function for mesonic (M) or baryonic (B) particle species i with mass M_i is given by,

$$\ln \mathcal{Z}_{M_i}^{M/B} = \mp \frac{V d_i}{2\pi^2} \int_0^\infty dk k^2 \ln(1 \mp z_i e^{-\varepsilon_i/T})$$

$$= \frac{VT^3}{2\pi^2} d_i \left(\frac{M_i}{T}\right)^2 \sum_{k=1}^\infty (\pm 1)^{k+1} \frac{z_i^k}{k^2} K_2(kM_i/T) \quad . \tag{7}$$

Here upper signs correspond to mesons and lower signs to baryons; $\varepsilon_i = \sqrt{k^2 + M_i^2}$ denotes the energy of particle i, d_i is its degeneracy factor and its fugacity is given by

$$z_i = \exp\left((B_i \mu_B + Q_i \mu_Q + S_i \mu_S)/T\right) \,. \tag{8}$$

With these relations it is straightforward to calculate susceptibilities and charge correlations in the HRG model using Eqs. (3) and (4).

We note that a HRG model is defined by specifying the resonance spectrum used to construct the partition function in Eq. (6). We use all hadron resonances with masses $M_H \leq 2.5$ GeV listed by the particle data group (PDG) in their 2010 summary tables[2] [28]. It is similar to that used, for example, in Ref. [11]. One question, that we will discuss in the comparison of lattice QCD results with HRG model calculations, is to what extent the strangeness sector is well represented in the HRG model calculations. This question has also been addressed in [11].

B. The ideal gas limit

In the infinite temperature limit, the grand canonical QCD partition function reduces to that of an ideal gas of quarks and gluons. In this limit, quark mass effects, including those in the strange quark sector, are negligible and we may compare our $(2+1)$-flavor QCD calculations with a free quark-gluon gas of 3-flavor QCD (Stefan-Boltzmann (SB) gas). This is given by [29]

$$\frac{p_{SB}}{T^4} = \frac{8\pi^2}{45} + \frac{7\pi^2}{20} + \sum_{f=u,d,s} \left[\frac{1}{2}\left(\frac{\mu_f}{T}\right)^2 + \frac{1}{4\pi^2}\left(\frac{\mu_f}{T}\right)^4\right] \,, \tag{9}$$

where the first two terms give the contributions of the gluon and the quark sectors for vanishing chemical potentials. After expressing the flavor chemical potentials in terms of μ_B, μ_Q and μ_S as given in Eq. (1), it is straightforward to read off the ideal gas values for diagonal and off-diagonal susceptibilities. These are listed in Table I.

III. LATTICE CALCULATIONS

In order to analyze fluctuations of conserved charges, we perform calculations on gauge field configurations generated in our study of the finite-temperature transition in $(2+1)$-flavor QCD [27]. These calculations were performed with

---

[2] In this summary table there are a few three starred resonances listed which do not have a known spin assignment. For these we use the minimal degeneracy factors. We also checked that the inclusion of some known heavier resonances as well as the inclusion of charmed hadrons does not alter the picture presented here. Moreover, we checked the stability of HRG results by reducing the mass cut-off from 2.5 GeV to 2.0 GeV. This alters the relevant observables discussed here by at most 2% at $T = 200$ MeV.

the HISQ/tree action for three values of the lattice cut-off corresponding to lattices with temporal extent $N_\tau = 6$, 8 and 12 and a spatial lattice extent $N_\sigma = 4N_\tau$. The calculations cover a temperature range, 130 MeV $\lesssim T \lesssim$ 350 MeV. In this temperature range the line of constant physics is defined by tuning the strange quark mass m_s to its physical value and setting the light quark masses to $m_l = m_s/20$, which correspond to a pion mass $M_\pi \simeq 160$ MeV.

It is important to note that the definition of physical quark and/or pion masses is not straightforward in calculations with staggered fermions at non-zero values of the lattice spacing due to taste symmetry breaking. Taste symmetry breaking, which is a consequence of the doubling problem in the staggered formulation, gives rise to sixteen pseudo-scalar mesons corresponding to the sixteen elements of the Clifford algebra, of which only one, with taste matrix γ_5, behaves as a Goldstone particle at finite lattice spacing. Even in the chiral limit, the other 15 modes receive masses of $\mathcal{O}(a^2)$ which vanish only in the continuum limit. Thus, as a result of taste symmetry breaking, these sixteen modes contribute to observables with different masses. The same is true of all other states, but the problem is most severe for Goldstone modes. The size of these effects has been quantified for the staggered fermion discretization scheme exploited here (HISQ/tree) by measuring the masses of the sixteen taste pions and by defining a root-mean-squared mass [27],

$$M_\pi^{RMS} = \frac{1}{4}\sqrt{M_{\gamma_5}^2 + M_{\gamma_0\gamma_5}^2 + 3M_{\gamma_i\gamma_5}^2 + 3M_{\gamma_i\gamma_j}^2 + 3M_{\gamma_i\gamma_0}^2 + 3M_{\gamma_i}^2 + M_{\gamma_0}^2 + M_1^2}. \tag{10}$$

Taste symmetry breaking also affects the generation of the ensemble of gauge configurations on which measurements are made. To simulate the desired number of flavors, the fourth-root of the staggered fermion determinant is taken for each flavor. While this "rooting" trick corrects for the number of flavors in the continuum limit, at finite lattice spacings, the masses of states contributing to the partition function are not degenerate.

With the improved staggered fermion action (HISQ/tree) used in our calculation, taste violations, while strongly suppressed, are still large [27]. In fact, our analysis showed that the HISQ/tree action has the smallest taste violations compared to the other improved staggered actions (p4, asqtad and stout) used in finite temperature calculations. Nevertheless, at values of the cut-off corresponding to the transition region ($T \simeq 160$ MeV) on the three different N_τ lattices analyzed by us, the RMS masses vary from $M_\pi^{RMS} \simeq 215$ MeV on our finest lattices ($N_\tau = 12$) to $M_\pi^{RMS} \simeq 415$ MeV on the coarsest lattice ($N_\tau = 6$), in contrast to the Goldstone pion mass 140 MeV [27]. We also find that, to a good approximation, the difference of M_π^{RMS} and the physical pion mass M_π is proportional to the square of the lattice cut-off at a fixed value of the temperature, $(aT)^2 \sim 1/N_\tau^2$. In this paper we show that the cut-off effects resulting from a much heavier RMS mass influence most strongly the electric charge fluctuations as these are most sensitive to the contributions from pions. It is worth pointing out, for comparison, that to obtain an RMS mass of about 215 MeV achieved with the HISQ/tree action on $N_\tau = 12$ lattices will require $N_\tau \approx 20$ with the asqtad and stout actions [21, 27].

We typically analyzed 10,000–20,000 gauge field configurations per parameter set for $N_\tau = 6$, 10,000–14,000 configurations for $N_\tau = 8$ and up to 6000 configurations for $N_\tau = 12$ lattices. Measurements of all operators needed to calculate quadratic fluctuations have been performed every 10 hybrid Monte Carlo time units for $N_\tau = 12$ and every 10 or 20 time units for $N_\tau = 6$, 8 lattices. Most of our quark number susceptibilities on the $N_\tau = 6$ and 8 lattices were calculated on GPU-clusters and we used 500–1500 random source vectors for the analysis. The $N_\tau = 12$ data were analyzed using 400 random source vectors at low temperatures and 100 at high temperatures.

When performing lattice QCD calculations at non-zero temperature, we have to control (at least) two different sources of cut-off errors. On the one hand there is the intrinsic cut-off dependence of the observables calculated at non-zero temperature at a certain value of the cut-off a^{-1}. We reduce these by working with tree-level $\mathcal{O}(a^2)$ improved actions in the gauge as well as the fermion sector. This improvement also insures that at high temperature the cut-off dependence of the basic operators entering our calculations is small. An additional cut-off dependence arises due to the choice of the zero temperature observable used to set the scale for all finite temperature measurements. We investigate two different scale-setting observables: the length scale r_1 extracted from the slope of the static quark potential,

$$\left(r^2 \frac{dV_{\bar{q}q}(r)}{dr}\right)_{r=r_1} = 1.0 \ , \tag{11}$$

and the kaon decay constant f_K. The temperature in these units is $T_{r_1}r_1 = r_1/(aN_\tau)$ and $T_{f_K}/f_K = 1/(f_KaN_\tau)$. The efficacy of these observables in setting the scale is complementary in many respects [27]. In particular, we note that r_1 has a mild dependence on the quark masses and is well defined even in the infinite quark mass limit. The kaon decay constant, on the other hand, has a sizeable quark mass dependence, and at lattice spacings used in this study, it is sensitive to taste symmetry violations in the hadron spectrum. To convert to physical units, we use $r_1 = 0.3106(20)$ fm [30] and the latest PDG value for the kaon decay constant, $f_K = 156.1/\sqrt{2}$ MeV. In Fig. 1, we show the difference in the two estimates of temperature over the interval relevant to the calculations performed here. The leading order correction contributing to this difference is $\mathcal{O}(g^2a^2)$.
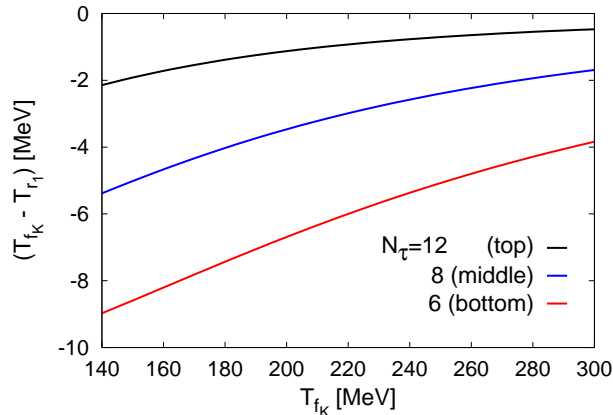
FIG. 1. Difference in temperature scales obtained from calculations of r_1 and f_K at values of the cut-off relevant for the temperature range explored in the calculation of quark number susceptibilities.
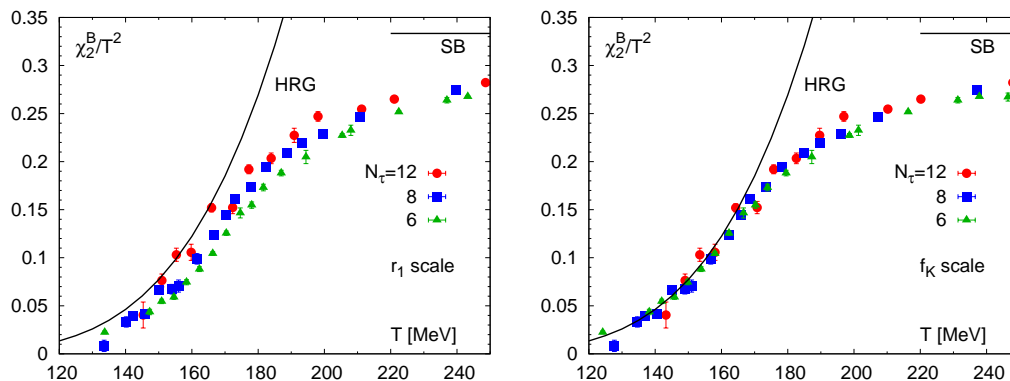

FIG. 2. Net baryon number fluctuations versus temperature. The left hand figure shows results using the potential shape parameter r_1 to set the scale for the temperature. The right hand figure shows the same data using f_K to set the scale. Also shown are the results obtain from the HRG model and the infinite temperature ideal gas limit (solid lines).

As noted in [27], we also find that in the study of charge fluctuations it is advantageous to use the f_K scale as it absorbs a significant fraction of the cut-off effects, *i.e.*, the cut-off effects are similar and cancel to a large extent in the ratio of hadron masses and temperature, M/T. However, it should be stressed that any one observable (r_1 or f_K) cannot eliminate cut-off effects in all observables equally well. We elaborate on this point in more detail in the appendix.

IV. FLUCTUATIONS

A. Fluctuations in baryon number, strangeness, and electric charge

We start our discussion of the fluctuations of baryon number, strangeness and electric charge by summarizing the data obtained on lattices with temporal extent $N_\tau = 6$, 8 and 12 in Tables II, III and IV and discussing their scaling behavior. The continuum extrapolation and comparison to the HRG model as well as the asymptotic high temperature ideal gas results are discussed in detail in the next subsection.

Figure 2 shows results for the baryon number susceptibility with the temperature scale set using r_1 (left hand panel) and f_K (right hand panel). In both cases, we show the results from the HRG model including all resonances with mass $M_H \leq 2.5$ GeV. The noticeable differences between the left and right hand panels of Fig. 2 are due to setting of the temperature scale and we find that the cut-off effects are smaller when a scale based on f_K is used. As

β	T (MeV)	χ_2^B/T^2	χ_2^Q/T^2	χ_2^S/T^2	χ_{11}^{BS}/T^2	χ_{11}^{BQ}/T^2	χ_{11}^{QS}/T^2
5.900	124.17	0.0223(15)	0.1173(7)	0.0601(6)	-0.0090(6)	0.0067(6)	0.0256(2)
6.000	138.22	0.0436(28)	0.1829(12)	0.1080(10)	-0.0207(11)	0.0114(9)	0.0437(3)
6.025	141.98	0.0545(22)	0.2037(16)	0.1241(14)	-0.0258(12)	0.0144(6)	0.0491(6)
6.050	145.83	0.0590(23)	0.2283(7)	0.1426(11)	-0.0283(14)	0.0154(6)	0.0572(4)
6.075	149.79	0.0745(26)	0.2551(14)	0.1672(14)	-0.0382(13)	0.0182(6)	0.0645(5)
6.100	153.85	0.0881(24)	0.2885(14)	0.1983(14)	-0.0472(13)	0.0205(6)	0.0756(4)
6.125	158.01	0.1044(19)	0.3216(18)	0.2317(19)	-0.0580(11)	0.0225(4)	0.0868(5)
6.150	162.28	0.1256(22)	0.3614(31)	0.2741(26)	-0.0729(15)	0.0264(4)	0.1006(9)
6.175	166.66	0.1466(52)	0.3956(32)	0.3200(54)	-0.0887(29)	0.0290(25)	0.1157(20)
6.195	170.25	0.1548(32)	0.4176(20)	0.3513(30)	-0.0987(23)	0.0280(5)	0.1263(6)
6.215	173.90	0.1730(34)	0.4427(25)	0.3937(38)	-0.1155(25)	0.0288(5)	0.1391(7)
6.245	179.52	0.1881(29)	0.4666(23)	0.4422(36)	-0.1324(20)	0.0278(5)	0.1549(10)
6.285	187.27	0.2048(68)	0.4978(30)	0.5116(64)	-0.1504(50)	0.0272(32)	0.1806(31)
6.341	198.61	0.2272(20)	0.5198(24)	0.5893(40)	-0.1845(17)	0.0214(2)	0.2024(13)
6.354	201.34	0.2326(53)	0.5261(25)	0.6098(72)	-0.1936(46)	0.0195(24)	0.2083(30)
6.423	216.33	0.2517(14)	0.5466(12)	0.6881(23)	-0.2212(13)	0.0152(1)	0.2334(7)
6.488	231.33	0.2639(28)	0.5586(15)	0.7420(43)	-0.2404(26)	0.0118(13)	0.2508(18)
6.515	237.81	0.2676(9)	0.5629(9)	0.7576(17)	-0.2472(9)	0.0102(1)	0.2552(5)
6.550	246.45	0.2672(41)	0.5678(19)	0.7787(54)	-0.2528(36)	0.0072(19)	0.2629(24)
6.664	276.43	0.2777(11)	0.5714(11)	0.8101(23)	-0.2667(11)	0.0055(1)	0.2717(5)
6.800	316.10	0.2806(18)	0.5718(10)	0.8248(36)	-0.2722(18)	0.0042(8)	0.2761(14)
6.950	365.18	0.2862(27)	0.5714(15)	0.8374(57)	-0.2794(26)	0.0034(14)	0.2790(21)
7.150	440.31	0.2803(23)	0.5666(12)	0.8395(43)	-0.2783(23)	0.0010(11)	0.2804(17)

TABLE II. Quadratic fluctuations of net baryon number, electric charge and strangeness as well as correlations among these conserved charges in units of T^2 calculated on lattices with temporal extent $N_\tau = 6$. We use f_K to define the temperature scale.

β	T (MeV)	χ_2^B/T^2	χ_2^Q/T^2	χ_2^S/T^2	χ_{11}^{BS}/T^2	χ_{11}^{BQ}/T^2	χ_{11}^{QS}/T^2
6.195	127.69	0.0083(58)	0.1377(19)	0.0690(13)	-0.0050(21)	0.0018(20)	0.0321(7)
6.245	134.64	0.0332(52)	0.1711(18)	0.0933(17)	-0.0151(23)	0.0090(16)	0.0391(7)
6.260	136.79	0.0390(28)	0.1868(20)	0.1054(11)	-0.0183(10)	0.0104(12)	0.0436(4)
6.285	140.45	0.0417(40)	0.2092(19)	0.1212(18)	-0.0198(20)	0.0110(11)	0.0507(3)
6.315	144.95	0.0668(38)	0.2455(23)	0.1490(31)	-0.0315(29)	0.0177(7)	0.0588(6)
6.341	148.96	0.0673(49)	0.2692(38)	0.1718(39)	-0.0345(29)	0.0164(12)	0.0686(7)
6.354	151.00	0.0705(63)	0.2908(23)	0.1878(31)	-0.0359(35)	0.0173(15)	0.0760(7)
6.390	156.78	0.0988(54)	0.3362(37)	0.2385(40)	-0.0557(31)	0.0215(11)	0.0914(10)
6.423	162.25	0.1235(28)	0.3811(15)	0.2894(23)	-0.0731(18)	0.0252(7)	0.1081(6)
6.445	165.98	0.1444(27)	0.4161(30)	0.3398(19)	-0.0919(15)	0.0263(8)	0.1239(11)
6.460	168.57	0.1610(24)	0.4287(19)	0.3623(30)	-0.1034(17)	0.0288(5)	0.1294(9)
6.488	173.49	0.1731(34)	0.4534(24)	0.4058(44)	-0.1170(28)	0.0281(4)	0.1444(10)
6.515	178.36	0.1948(24)	0.4794(28)	0.4606(35)	-0.1390(19)	0.0279(5)	0.1608(11)
6.550	184.84	0.2085(17)	0.5034(19)	0.5177(30)	-0.1572(13)	0.0257(4)	0.1803(10)
6.575	189.58	0.2190(17)	0.5171(10)	0.5586(19)	-0.1719(13)	0.0236(2)	0.1933(4)
6.608	196.01	0.2291(23)	0.5321(18)	0.6052(39)	-0.1874(22)	0.0209(1)	0.2089(10)
6.664	207.32	0.2465(22)	0.5511(13)	0.6711(35)	-0.2123(20)	0.0171(2)	0.2294(8)
6.800	237.07	0.2748(14)	0.5786(14)	0.7796(27)	-0.2540(13)	0.0104(1)	0.2628(7)
6.950	273.88	0.2901(7)	0.5963(10)	0.8443(18)	-0.2782(7)	0.0060(1)	0.2831(5)
7.150	330.23	0.2984(5)	0.6073(9)	0.8829(13)	-0.2919(5)	0.0032(1)	0.2955(4)

TABLE III. Same as Table II but for $N_\tau = 8$.

| β	T (MeV)	χ_2^B/T^2	χ_2^Q/T^2	χ_2^S/T^2	χ_{11}^{BS}/T^2	χ_{11}^{BQ}/T^2	χ_{11}^{QS}/T^2
6.70	143.25	0.0404(135)	0.2741(64)	0.1586(53)	-0.0227(59)	0.0088(65)	0.0679(33)
6.74	149.03	0.0764(67)	0.3178(52)	0.1939(46)	-0.0348(40)	0.0208(32)	0.0796(25)
6.77	153.48	0.1031(68)	0.3492(86)	0.2365(59)	-0.0581(42)	0.0225(34)	0.0892(33)
6.80	158.05	0.1056(83)	0.3721(46)	0.2663(53)	-0.0632(47)	0.0212(40)	0.1015(27)
6.84	164.31	0.1520(42)	0.4358(45)	0.3531(59)	-0.0975(30)	0.0272(20)	0.1278(22)
6.88	170.77	0.1522(64)	0.4471(40)	0.3808(66)	-0.1009(46)	0.0257(30)	0.1399(30)
6.91	175.76	0.1920(46)	0.4943(36)	0.4650(63)	-0.1361(42)	0.0280(21)	0.1645(28)
6.95	182.59	0.2034(55)	0.5030(59)	0.5067(90)	-0.1506(55)	0.0264(28)	0.1780(46)
6.99	189.64	0.2273(73)	0.5273(69)	0.5779(87)	-0.1820(66)	0.0227(35)	0.1979(48)
7.03	196.91	0.2470(49)	0.5483(36)	0.6319(87)	-0.2006(45)	0.0232(24)	0.2157(34)
7.10	210.21	0.2547(33)	0.5671(27)	0.7004(106)	-0.2213(38)	0.0167(16)	0.2395(30)
7.15	220.15	0.2650(25)	0.5744(26)	0.7389(44)	-0.2366(32)	0.0142(12)	0.2512(24)
7.28	247.91	0.2822(19)	0.5902(15)	0.8063(37)	-0.2646(22)	0.0088(8)	0.2708(15)

TABLE IV. Same as Table II but for $N_\tau = 12$.
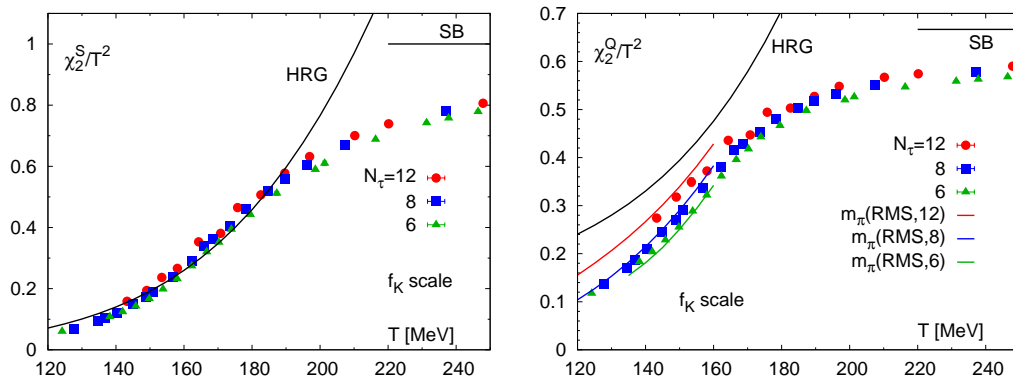
FIG. 3. Net strangeness (left) and net electric-charge (right) fluctuations versus temperature obtained from lattice calculations at three different values of the lattice cut-off $aT = 1/N_\tau$. Calculations of f_K have been used to fix the temperature scale. Also shown are the results obtained from the HRG model and the infinite temperature ideal gas limit (solid lines) as well as three short, solid lines for a HRG model in which the pion mass has been replaced by the RMS pion mass relevant for our calculations on the $N_\tau = 6$, 8 and 12 lattices, respectively.

pointed out above, this feature has also been noted in the analysis of chiral observables [27, 31]. In principle, both scales should lead to identical results in the continuum limit, however, the continuum extrapolation is much better controlled when the cut-off effects are small. We therefore use the f_K temperature scale in the rest of the paper unless stated otherwise.

In Fig. 3, we show results for fluctuations of net strangeness (left) and net electric charge (right) using f_K to set the scale for the temperature. The figure also shows the corresponding HRG results. Both, the strangeness and the baryon number (see Fig. 2) fluctuations agree with HRG results for temperatures below $T \simeq 160$ MeV and show small cut-off effects. The electric charge fluctuations deviate significantly from HRG results at all temperatures and show large cut-off dependence. These large cut-off effects in $\hat{\chi}_2^Q$ can mostly be explained as due to discretization errors in the lattice hadron spectrum. The dominant contribution to $\hat{\chi}_2^Q$ at low temperatures comes from pions, while $\hat{\chi}_2^S$ receives the leading contribution from kaons and $\hat{\chi}_2^B$ from nucleons. As discussed in Section III, the pion spectrum is strongly affected by taste symmetry violations in the staggered formulation, and it has been shown in earlier work that the agreement in $\hat{\chi}_2^Q$ between lattice QCD results and HRG model calculations can be improved using a distorted spectrum in the HRG analysis [32, 34].

To confirm this observation, we show in Fig. 3 (right panel) the HRG results obtained after replacing the physical pion mass by the RMS pion mass relevant to our calculations on the $N_\tau = 6$, 8 and 12 lattices, respectively. These cut-off effects leading to the spectral distortion vary not only with N_τ but also with temperatures at fixed N_τ. We therefore parametrize the cut-off dependence of M_π^{RMS}, at each N_τ, using a cubic polynomial fit to the data given

in [27]. This allowed us to estimate the modified HRG result as a function of temperature, as shown in Fig. 3 by short solid lines (colored lines). The data confirm that below $T \simeq 155$ MeV, the numerical results for $\hat{\chi}_2^Q$ are well described by this minimally modified HRG model and the major part of the difference is indeed due to the taste symmetry breaking effects in the pion sector. Since all other heavier states contributing to the HRG model are assumed to take on their physical values, the fluctuations of strangeness and baryon number are not influenced by this modification of the HRG model. We discuss these features, together with continuum extrapolations, for the data shown in Fig. 2 and 3 in more detail in the following subsection.

It is worthwhile to clarify our discussion of the comparison of lattice QCD data with the HRG model. When we say that the HRG is a good approximation to QCD, we refer to the value of the susceptibility, as is traditional. At the temperature where this agreement fails, we observe that not only the value but the slope also deviates significantly. Our data also indicate that the curvature starts to deviate 20–30 MeV earlier depending on the observable. These derivatives of the susceptibility are related to higher moments, which are increasingly less well captured in the HRG analysis and have not been calculated in our lattice simulations.

B. Continuum extrapolation and approach to the hadron resonance gas estimates

In this section, we analyze cut-off effects at fixed values of the temperature for three values of the lattice spacing, $aT = 1/6$, $1/8$ and $1/12$. We perform this analysis for temperature scales defined in terms of both r_1 and f_K in order to quantify systematic effects at a given lattice spacing and to demonstrate consistency between the estimates in the continuum limit. Our simulations on the lattices with the three different N_τ values have not been done at the same values of the temperature. As a result, in order to perform continuum extrapolations at fixed temperature, we have used cubic spline interpolations of our data throughout this paper. We propagate errors on the spline parameters. In addition to estimating statistical errors based on our entire data sample, we also use the difference of spline interpolations performed on two independent sub-sets constructed by choosing every second T-point (even and odd points), as an estimate for the systematic errors. The final error on our data is obtained by adding this error estimate and the purely statistical error obtained from the full data set in quadrature.

We first discuss the continuum extrapolation for the three susceptibilities shown in Figs. 2 and 3 at high temperature, $T \geq 170$ MeV. In this regime, cut-off effects are generally small, which, to some extent, is due to the fact that our numerical calculations have been performed with an $\mathcal{O}(a^2)$ improved action with small cut-off dependence of thermodynamic observables in the infinite temperature ideal gas limit [33]. In Fig. 4, we show continuum extrapolations for all three susceptibilities, $\chi_2^{S,Q,B}$, at three representative values of the temperature, $T = 170$, 190 and 210 MeV. In each case, and for both temperature scales, r_1 and f_K, the fits show that the cut-off effects are consistent with $\mathcal{O}(g^2(aT)^2)$ corrections and, over the limited range of T, all three susceptibilities can be extrapolated to the continuum with an Ansatz that includes corrections linear in $1/N_\tau^2 = (aT)^2$. The continuum extrapolated results obtained with the two temperature scales agree within errors, and the results obtained on the $N_\tau = 12$ lattices are a good approximation to these. This also is true for lower temperatures. However, in this case extrapolations linear in $1/N_\tau^2$ are no longer sufficient for the electric charge and strangeness fluctuations. Systematic effects at $\mathcal{O}((aT)^4)$ start to become important. This is evident from the data sets at $T = 150$ MeV, which are shown in Fig. 4 as well. We note that also at this temperature, which is the lowest temperature for which we perform continuum extrapolations, extrapolations based on the r_1 and f_K temperature scales are in good agreement. Having demonstrated consistency of the continuum estimate obtained using r_1 and f_K, we, as stated previously, use the scale from f_K in the rest of the paper because the slope in the fits is smaller.

The data for the net charge fluctuations in the temperature interval 120–250 MeV, results of the linear extrapolation for χ_2^B/T^2, and quadratic extrapolations for χ_2^S/T^2 and χ_2^Q/T^2 are shown in Figs. 5 and 6. In Fig. 6(right) we also show the ratio of net baryon number and electric charge fluctuations. The continuum extrapolation shown for this quantity has been obtained from the corresponding extrapolations for χ_2^B/T^2 and χ_2^Q/T^2.

Continuum extrapolations in the crossover and the low temperature regions require additional considerations because the three different conserved charge susceptibilities show different sensitivities to cut-off effects. In order to quantify differences from the HRG model results in this temperature regime, and in order to clarify the extent to which the HRG model provides a good description of QCD results, we analyze the ratios $\chi_2^X/\chi_2^{X,HRG}$, $X = B$, Q, and S, in Fig. 7. We find that, while baryon number fluctuations start to agree with HRG model results for $T \lesssim 165$ MeV, the net strangeness fluctuations become larger than the HRG values for temperatures below $T \simeq 190$ MeV and then approach the HRG values from above at $T \lesssim 150$ MeV. At $T \sim 150$ MeV, the differences are still (10-20)%.

The electric charge fluctuations show much larger deviations from the HRG model as is evident from Fig. 7. In particular, below $T \simeq 170$ MeV, the cut-off dependence in $\chi_2^Q/\chi_2^{Q,HRG}$ is large and extrapolations including just leading order a^2-corrections fail. As discussed in Section IV A, this, to a large extent, is due to the severe cut-off
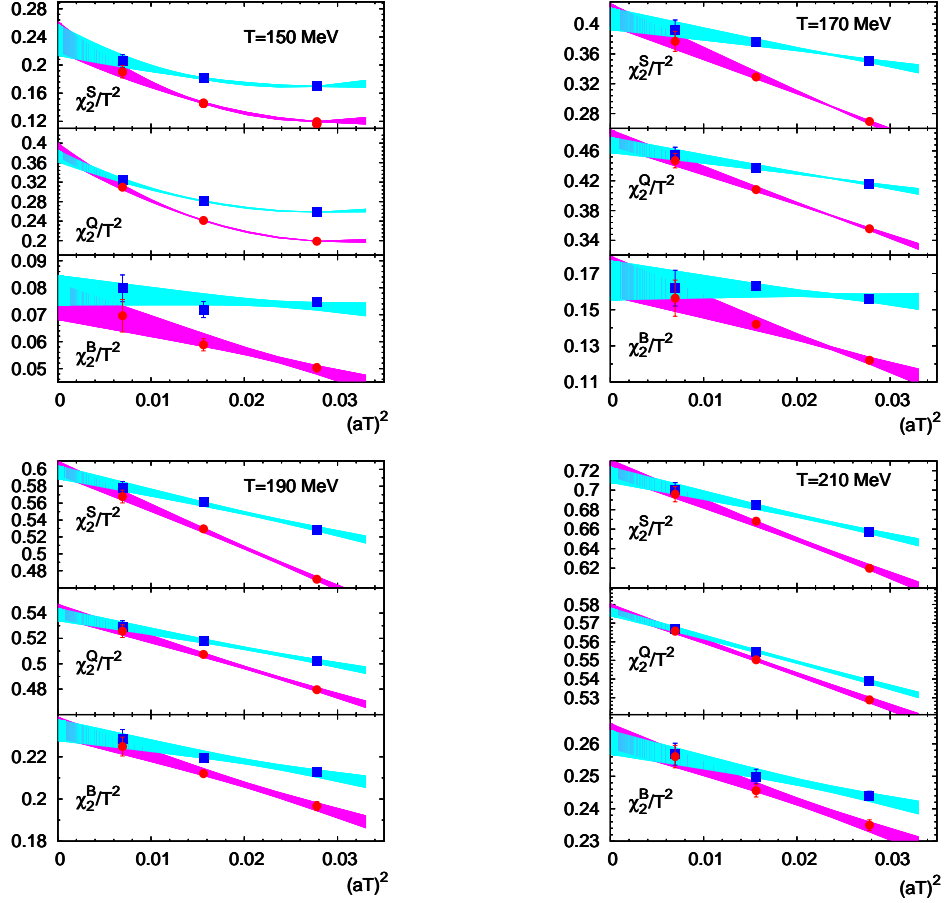
FIG. 4. Continuum extrapolations of net strangeness (χ_2^S/T^2), net electric charge (χ_2^Q/T^2) and net baryon number (χ_2^B/T^2) at four values of the temperature using fits linear and, for χ_2^S/T^2 and χ_2^Q/T^2, at the lowest temperature quadratic in $(aT)^2 = 1/N_\tau^2$.
Data at fixed values of the temperature are obtained from cubic spline interpolations. The temperature scale has been determined using calculations of r_1 (circles) and f_K (boxes), respectively.

dependence of the pion spectrum, *i.e.*, the anomalously large RMS pion mass suppresses fluctuations in the electric charge and has a much smaller effect on the baryon and strangeness charges. In short, a continuum extrapolation without including the effects of taste symmetry breaking is insufficient.

The distorted HRG model, which modifies the log of the partition function by replacing M_π by M_π^{RMS} in the pion contribution, $\exp(-M_\pi/T)$, however, does describe the data well. In general, the HRG model defined in Eq. 7 suggests that, in this temperature regime, cut-off effects in any quantity f may be accounted for by an exponential Ansatz of the form

$$f(N_\tau, T) = a(T) + b(T)\, e^{-c(T)/N_\tau^2} \,, \tag{12}$$

which, at high temperatures where cut-off effects become small, reduces to the linear fit in $1/N_\tau^2$, *i.e.*, $f(N_\tau, T) \simeq \tilde{a}(T) + \tilde{b}(T)/N_\tau^2$ and also incorporates the next to leading order quadratic corrections $f(N_\tau, T) \simeq \tilde{a}(T) + \tilde{b}(T)/N_\tau^2 + \tilde{c}(T)/N_\tau^4$. We, therefore, analyze our data for $\hat{\chi}_2^{Q,S}$ in the transition region, $150 \le T \le 190$ MeV, from the low to high temperature phase of (2+1)-flavor QCD using fits linear and quadratic in $1/N_\tau^2$ as well as the exponential Ansatz given in Eq. (12). With our current statistical accuracy we are, however, not sensitive to cut-off effects beyond $\mathcal{O}((aT)^4)$. In fact, all our fits performed with the exponential ansatz are consistent within errors with fits based on the quadratic ansatz. We, therefore, do not discuss the exponential fits any further in this paper. In the case of $\hat{\chi}_2^B$ we find that linear and quadratic fits agree within errors and lead to a χ^2/dof less than unity in the entire range of temperatures $T \ge 150$ MeV. We therefore use the linear fits to perform continuum extrapolations for $\hat{\chi}_B$. For strangeness and electric charge susceptibilities we use quadratic extrapolations in the entire temperature range, although, as discussed above, we do not observe systematic differences between linear and quadratic extrapolations for
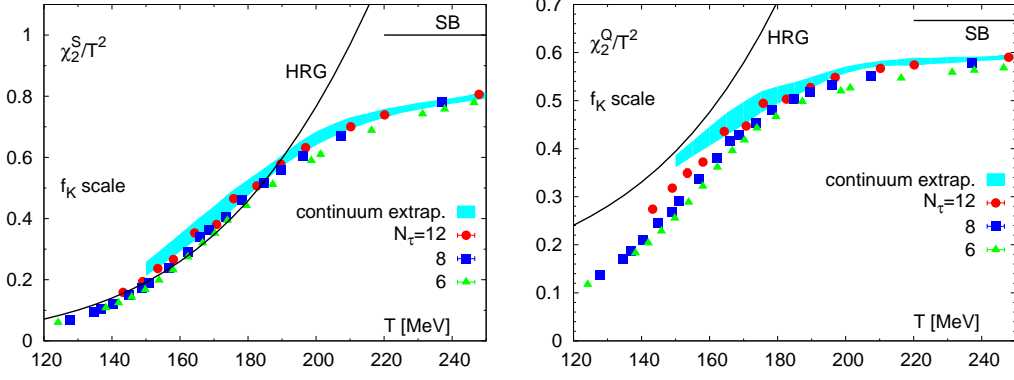
FIG. 5. Fluctuations of net strangeness (left) and electric charge (right) in units of T^2. Calculations of f_K have been used to fix the temperature scale. Also shown are continuum extrapolated results taking into account cut-off effects up to quadratic order in $1/N_\tau^2$. The HRG model result and the SB limit is given by the solid lines.
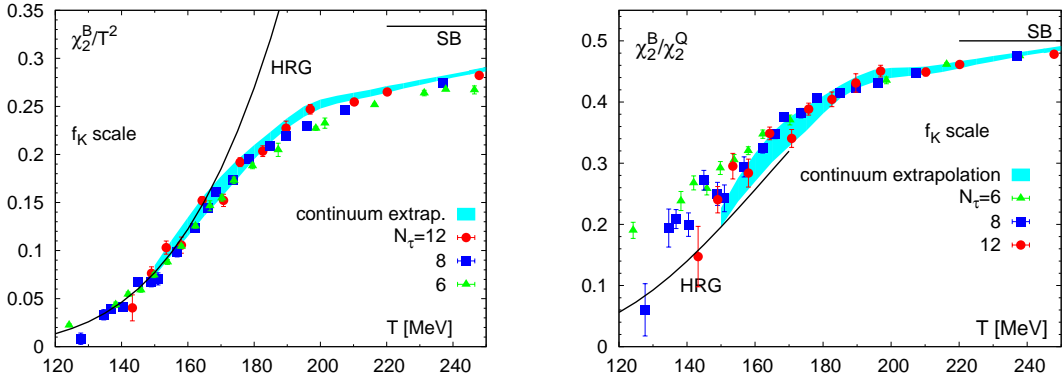

FIG. 6. Net baryon number fluctuations in units of T^2 (left) and the ratio of net baryon number and net electric charge fluctuations (right). Calculations of f_K have been used to fix the temperature scale. Also shown are results from a continuum extrapolation taking into account $\mathcal{O}(a^2)$ corrections. For χ_2^B/χ_2^Q we also show the ratio of continuum extrapolations constructed for χ_2^B/T^2 and χ_2^Q/T^2 separately. The HRG model result and the SB limit is given by the solid lines.

$T \gtrsim 170$ MeV. Using the latter for our continuum extrapolations, however, leads to more conservative error estimates.

A summary of our continuum extrapolations for $\chi_2^X/\chi_2^{X,HRG}$ and the data in the low temperature region is also shown in Fig. 7. Due to taste symmetry breaking, the data show significant dependence on N_τ for $T \lesssim 170$ MeV. To understand this cut-off effect we compare, in the bottom panel in Fig. 7, results for $\chi_2^Q/\chi_2^{Q,HRG}$ with a modified HRG model in which the physical pion mass is replaced by (i) the N_τ dependent RMS mass, $\mathrm{HRG}(M_\pi^{\mathrm{RMS}})/\mathrm{HRG}(M_\pi^{\mathrm{physical}})$, and (ii) a pion mass of 160 MeV, $\mathrm{HRG}(M_\pi = 160\ \mathrm{MeV})/\mathrm{HRG}(M_\pi^{\mathrm{physical}})$, corresponding to the light quark mass actually used in our calculations. Since the line showing $\mathrm{HRG}(M_\pi = 160\ \mathrm{MeV})/\mathrm{HRG}(M_\pi^{\mathrm{physical}})$ is much closer to unity compared to the other three, we confirm that the errors due to simulating at this slightly heavier pion mass are significantly smaller than the cut-off effects leading to a much heavier RMS mass.

In the interesting temperature range relevant to the discussion of freeze-out conditions in heavy ion collisions, 160 MeV $\lesssim T \lesssim 170$ MeV, we find that the continuum extrapolated electric charge fluctuations are (10-20)% smaller than even the modified HRG model calculation with $M_\pi = 160$ MeV. For temperatures $T \lesssim 150$ MeV, the χ_2^Q data start to agree with the modified HRG results with $M_\pi = M_\pi^{\mathrm{RMS}}$ and continuum extrapolations using the quadratic Ansatz start to agree with the HRG result.

Strangeness fluctuations on the other hand, both for the $N_\tau = 12$ data and the continuum extrapolated values, stay systematically above the hadron resonance gas result in the temperature range 150–190 MeV. We, therefore, expect this feature to survive the continuum extrapolation. Below $T \lesssim 150$ MeV, fluctuations in the strangeness charge show
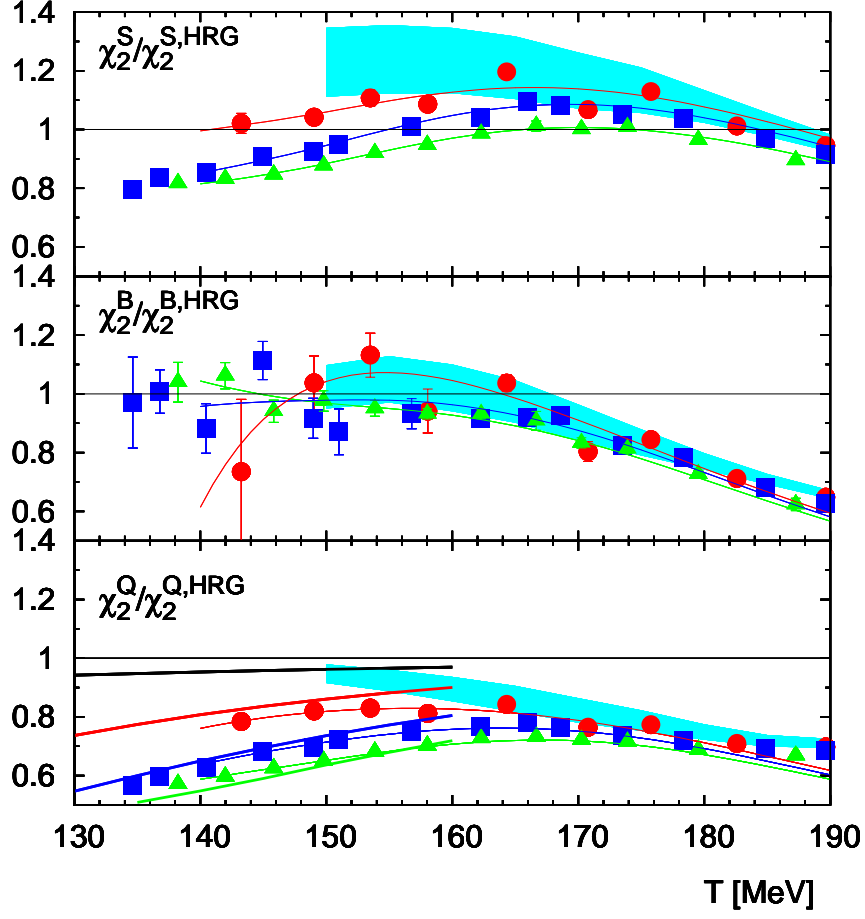
FIG. 7. Deviations of $\chi_2^{S,B,Q}$ from HRG model results. Data on $N_\tau = 6$, 8 and 12 lattices are shown using triangles, boxes and circles, respectively. Thin lines are the result of a cubic spine interpolation of the data at fixed N_τ. The broad bands are the result of the continuum extrapolations. In the bottom panel, the thick black line just below unity is the ratio HRG($M_\pi = 160$ MeV)/HRG($M_\pi^{\mathrm{physical}}$). The other thick lines show the ratio HRG(M_π^{RMS})/HRG($M_\pi^{\mathrm{physical}}$) for each of the three N_τ lattices.

an N_τ dependence, which is most likely again due to taste symmetry violations. More data are required to study this issue further.

Net baryon number fluctuations are consistent with HRG model results for temperatures below $T \simeq 160$ MeV, although statistical errors on our $N_\tau = 12$ data set make the quantification of possible deviations from the HRG result in this temperature range difficult. For larger values of the temperature, the estimates and errors in them grow progressively smaller. Our linear extrapolations suggest that in the temperature interval 160 MeV$\lesssim T \lesssim$170 MeV, deviations from the HRG model calculations are at most 10%. A confirmation of this in our data, through the inclusion of quadratic corrections, however, requires better statistics. Data obtained with the stout action [21] also suggest that the χ_2^B stays close to the HRG model result in this temperature range.

In order to reflect the influence of systematic effects on our continuum extrapolation we varied fit ranges and distribution of knots in the smooth spline interpolation. Moreover, in order to account for possible underestimates of errors on the individual data points, we divided our data samples into two independent sub-sets consisting of even and odd T-values by rank-order. We used the differences in these fits and the fit to the full data sample as an additional error on our spline interpolations.

To summarize, our continuum extrapolated values of $\chi_2^{B,Q,S}/T^2$ are given in Table V. Extrapolations of $\chi_2^{Q,S}/T^2$ used the Ansatz, Eq. (12) truncated at $O(1/N_\tau^4)$, i.e., we used the quadratic extrapolations, whereas for χ_2^B/T^2 the exponential was truncated at $O(1/N_\tau^2)$, i.e., we used the linear extrapolations. For $\chi_2^{Q,S}/T^2$ we also find that the quadratic extrapolated values agree with the exponential Ansatz. Our extrapolated results are in good agreement

T [MeV]	χ_2^B/T^2	χ_2^Q/T^2	χ_2^S/T^2	χ_{11}^{BS}/T^2	χ_{11}^{BQ}/T^2	χ_{11}^{QS}/T^2
150	0.0790(57)	0.3736(126)	0.2358(225)	-0.0415(60)	0.0187(29)	0.0929(61)
155	0.1026(77)	0.3998(158)	0.2770(260)	-0.0587(69)	0.0221(24)	0.1031(68)
160	0.1247(98)	0.4258(198)	0.3208(289)	-0.0767(75)	0.0242(23)	0.1173(70)
165	0.1470(109)	0.4513(232)	0.3645(322)	-0.0949(81)	0.0259(21)	0.1332(78)
170	0.1662(111)	0.4734(240)	0.4067(334)	-0.1115(84)	0.0269(21)	0.1491(84)
175	0.1849(99)	0.4964(222)	0.4567(314)	-0.1304(79)	0.0270(19)	0.1655(83)
180	0.2024(74)	0.5118(179)	0.5013(259)	-0.1497(66)	0.0263(17)	0.1782(77)
185	0.2182(56)	0.5239(144)	0.5449(215)	-0.1682(57)	0.0249(19)	0.1892(76)
190	0.2326(52)	0.5379(115)	0.5888(181)	-0.1860(56)	0.0233(22)	0.2005(72)
195	0.2445(55)	0.5522(84)	0.6289(210)	-0.2005(60)	0.0220(21)	0.2122(68)
200	0.2524(46)	0.5638(68)	0.6623(222)	-0.2116(52)	0.0205(21)	0.2235(70)
205	0.2570(41)	0.5717(57)	0.6884(210)	-0.2200(38)	0.0186(18)	0.2335(67)
210	0.2604(38)	0.5770(55)	0.7113(194)	-0.2267(31)	0.0168(15)	0.2424(62)
215	0.2637(36)	0.5792(63)	0.7282(155)	-0.2335(32)	0.0152(14)	0.2486(51)
220	0.2676(35)	0.5809(84)	0.7438(148)	-0.2397(35)	0.0140(12)	0.2537(57)
225	0.2713(28)	0.5824(63)	0.7565(113)	-0.2456(34)	0.0128(12)	0.2576(56)
230	0.2749(27)	0.5841(64)	0.7672(116)	-0.2511(33)	0.0119(12)	0.2606(56)
235	0.2784(23)	0.5855(56)	0.7760(105)	-0.2564(28)	0.0109(10)	0.2628(48)
240	0.2819(20)	0.5873(46)	0.7847(92)	-0.2613(24)	0.0101(8)	0.2649(39)
245	0.2852(20)	0.5890(45)	0.7934(98)	-0.2664(23)	0.0093(8)	0.2667(37)
250	0.2885(20)	0.5907(45)	0.8020(98)	-0.2710(23)	0.0085(7)	0.2688(34)

TABLE V. Continuum extrapolated results for the quadratic fluctuations of net baryon number, electric charge and strangeness densities and the correlations among them. Results for χ_2^Q/T^2 and χ_2^S/T^2 are obtained from quadratic fits and those for χ_2^B/T^2 from linear fits.

with the recently published analysis using the stout action [21].

Lastly, in Fig. 6 (right), we show the ratio of the net baryon number and electric charge fluctuations, χ_2^B/χ_2^Q. It approaches the HRG model result from above and starts to agree with it for $T \lesssim 150$ MeV. The continuum extrapolation here is based on the linear and exponential extrapolations for χ_2^B and χ_2^Q, respectively. In the region of interest to heavy ion phenomenology, this ratio varies between $0.29(4)$ (at 160 MeV) and $0.35(4)$ (170 MeV). Thus, fluctuations in net electric charge could be 3–4 times larger than in the net baryon number in the vicinity of the freeze-out temperature.

V. CORRELATIONS

Probes of the structure of QCD at finite temperature include correlations among different conserved charges. These correlations show characteristic changes in the crossover region between the low and high temperature phases of QCD, which are correlated with changes in the relevant degrees of freedom. They also provide insight into the applicability of HRG model calculations at low temperatures. The change in correlations between baryon number and electric charge, $\hat{\chi}_{11}^{BQ}$, is expected to be particularly striking as one goes from the low to the high temperature phase. At low temperatures this correlation is dominated by the contribution of protons plus anti-protons. Consequently, within the HRG model it rises exponentially with temperature in this region. In the high temperature limit of (2+1)-flavor QCD, however, $\hat{\chi}_{11}^{BQ}$ vanishes as the quarks become effectively massless, $(m_i/T \to 0)$, and the weighted sum of the charges of up, down and strange quarks vanishes. Results for $\hat{\chi}_{11}^{BQ}$ shown in Fig. 8 are consistent with this picture.

The correlations of strangeness with the baryon number and the electric charge, $\hat{\chi}_{11}^{BS}$ and $\hat{\chi}_{11}^{QS}$, are sensitive to changes in the strangeness degrees of freedom [22, 35, 36]. Results for the temperature dependence of these correlations are shown in Fig. 9. They approach the Stefan-Boltzmann value, 1/3, of a massless three flavor quark gas at high temperatures. As observed in the case of the quadratic fluctuations, on decreasing the temperature towards the transition region, these correlations first overshoot the HRG model result and then approach HRG value from above
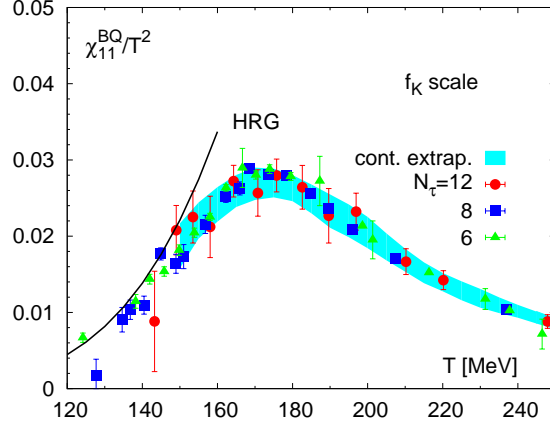
FIG. 8. Correlations of electric charge with baryon number versus temperature. The temperature scale has been set using f_K. The solid line shows the result for the HRG model. The band shows continuum extrapolations that take into account cut-off effects linear in $1/N_\tau^2$.
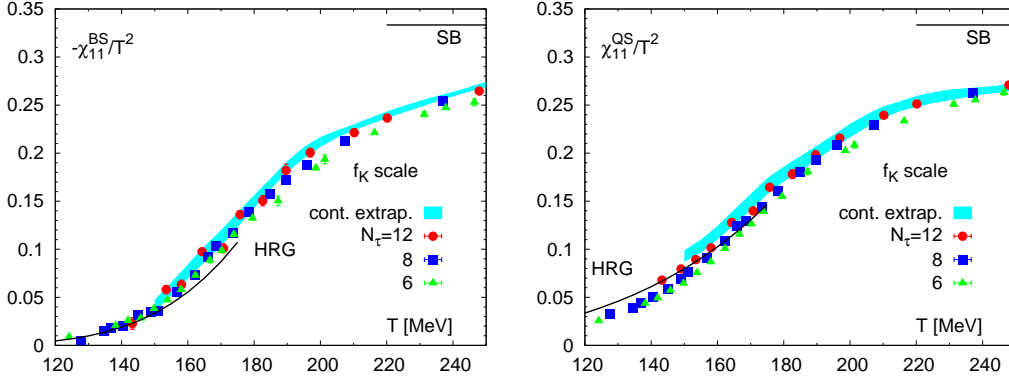

FIG. 9. Correlations of strangeness with baryon number (left) and electric charge (right). In both cases, f_K has been used to set the scale. The solid lines show the result for the HRG model. For χ_{11}^{BS}/T^2 the band shows continuum extrapolations that take into account cut-off effects linear in $1/N_\tau^2$ while for χ_{11}^{QS}/T^2 also quadratic corrections have been accounted for.

at about 150 MeV. This overshoot is more pronounced for $-\hat{\chi}_{11}^{BS}$ than for $\hat{\chi}_{11}^{QS}$. Also shown in Fig. 9 are continuum extrapolations (bands) which in the baryon sector, i.e., for B-S and B-Q correlations, are based on fits linear in $1/N_\tau^2$, whereas in the meson sector, i.e., for Q-S correlations, quadratic corrections are also taken into account. This reflects the larger sensitivity of the latter to taste violations that also has been observed for the quadratic strangeness and electric charge fluctuations.

In the isospin symmetric case considered in this study, the flavor correlations $\hat{\chi}_{11}^{us}$ and $\hat{\chi}_{11}^{ds}$ are equal. Also, the two correlations $2\hat{\chi}_{11}^{QS}$ and $\hat{\chi}_{11}^{BS}$ are related to each other through the quadratic strangeness fluctuations, i.e., $2\hat{\chi}_{11}^{QS} - \hat{\chi}_{11}^{BS} = \hat{\chi}_2^S$ [36]. One can then write the following relationships between the charge correlations and quark-flavor fluctuations:

$$\hat{\chi}_{11}^{QS} = \frac{1}{3}\left(\hat{\chi}_2^s - \hat{\chi}_{11}^{us}\right) \ ,$$
$$\hat{\chi}_{11}^{BS} = -\frac{1}{3}\left(\hat{\chi}_2^s + 2\hat{\chi}_{11}^{us}\right) \ . \tag{13}$$

At high temperatures $\hat{\chi}_{11}^{QS} \sim -\hat{\chi}_{11}^{BS}$ because $\hat{\chi}_{11}^{us}$ receives perturbative contributions only at $\mathcal{O}(g^6 \ln(1/g^2))$ and is therefore small [23, 37]. On the other hand, corrections to $\hat{\chi}_2^s$ from the ideal gas limit are dominant as they are $\mathcal{O}(g^2)$.

All three charge correlations show significant deviations from the ideal gas limit even at twice the transition temperature (see data in Tables II, III and IV). These deviations are due to large contributions of flavor fluctuations, such as to $\hat{\chi}_2^s$ discussed above. The leading order perturbative correction can be eliminated by forming suitable ratios
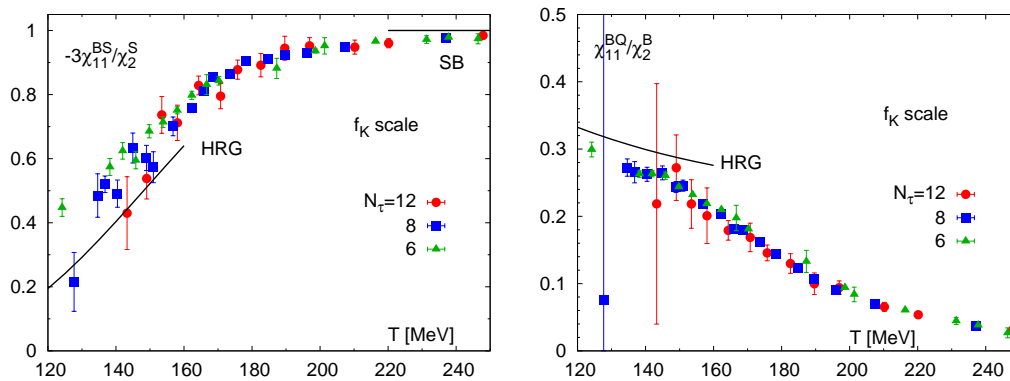
FIG. 10. Correlations between baryon number and strangeness (left) as well as electric charge (right) normalized to strangeness and net baryon number fluctuations, respectively. The solid line shows the HRG model result.

that can be used to analyze experimental data on charge fluctuations [22, 35, 36],

$$
C_{BS} = -3 \frac{\chi_{11}^{BS}}{\chi_2^S} \ ,
$$
$$
C_{QS} = 3 \frac{\chi_{11}^{QS}}{\chi_2^S} = \frac{1}{2} \left(3 - C_{BS}\right) \ . \tag{14}
$$

At high temperature the deviations from the ideal gas value of unity are now due to χ_{11}^{us}/χ_2^s, for example, $C_{BS} = 1 + 2\chi_{11}^{us}/\chi_2^s$. Data for C_{BS} is shown in Fig. 10(left) and, in comparison to the quadratic strangeness fluctuations (Fig. 3) or baryon number strangeness correlations (Fig. 9), the approach to the ideal gas limit is much more rapid. This shows that the flavor correlation $2\chi_{11}^{us}/\chi_2^s$ is already small for $T \gtrsim 1.2 T_c$. It is, however, large in the vicinity of the transition temperature.

The behavior of the third ratio that one can analyze, $C_{BQ} = \chi_{11}^{BQ}/\chi_2^B$, is somewhat different as leading order perturbative corrections do not cancel completely due to differences in the light and strange quark masses. Consequently, the approach to the ideal gas limit is slower as can be seen in Fig. 10(right).

VI. DISCUSSION AND CONCLUSION

We have analyzed quadratic fluctuations and correlations among conserved charges in (2+1)-flavor QCD. We find that as the temperature is decreased from the high temperature phase, the net baryon number fluctuations start to agree with the hadron resonance gas model below 165 MeV while for electric charge fluctuations this happens only below 150 MeV. The fluctuations of net strangeness overshoot the HRG model values at $T \sim 190$ MeV. In the temperature range relevant to the discussion of chemical freeze-out in heavy ion collisions, 160–170 MeV, strangeness fluctuations are systematically larger than the HRG model result by about 20%. These detailed differences between QCD calculations and HRG model results should become manifest when experimental data on the probability distributions of net charge fluctuations [2] is analyzed. In fact, quadratic fluctuations characterize the bulk structure of these distributions which, in the Gaussian approximation at $\mu_B = 0$, is given by

$$
P(N_X) = e^{-N_X^2/(2V_f T_f^3 \hat{\chi}_2^X)} \ , \quad X = B, \ S, \ Q \ , \tag{15}
$$

where T_f denotes the temperature at the time of chemical freeze-out and V_f is the freeze-out volume. The results presented here suggest that the largest deviations from HRG model calculations occur in the probability distributions for electric charge and strangeness fluctuations. We give a summary of the fluctuations in conserved charges for temperatures in the transition region in Table VI.

In the phenomenologically interesting temperature regime 160 MeV $\lesssim T \lesssim$ 170 MeV, continuum extrapolated results for $\hat{\chi}_2^Q$, are smaller than the HRG model results by about 10–20%. Even though at temperatures below 150 MeV, estimates for electric charge fluctuations have large systematic errors due to the distortion of the light meson spectrum in all staggered formulations, our analysis shows that these effects can be taken into account when performing

T [MeV]	$\chi_2^B/\chi_2^{B,HRG}$	$\chi_2^Q/\chi_2^{Q,HRG}$	$\chi_2^S/\chi_2^{S,HRG}$	$\chi_2^{BS}/\chi_2^{BS,HRG}$	$\chi_2^{BQ}/\chi_2^{BQ,HRG}$	$\chi_2^{QS}/\chi_2^{QS,HRG}$
155	1.049(79)	0.924(36)	1.240(116)	1.353(159)	0.804(86)	1.139(74)
160	1.020(80)	0.895(41)	1.235(111)	1.384(135)	0.717(67)	1.144(68)
165	0.972(72)	0.861(44)	1.212(106)	1.356(116)	0.633(51)	1.150(67)
170	0.898(60)	0.818(41)	1.171(96)	1.280(96)	0.544(42)	1.144(64)

TABLE VI. Quadratic fluctuations of net baryon number (δN_B), electric charge (δN_Q) and strangeness (δN_S) densities and correlations among these conserved net charges in the crossover region from the low to high temperature regime of QCD. We give results for quadratic fluctuations and correlations calculated in QCD relative to the corresponding HRG model results.

continuum extrapolations. We show that the resulting continuum estimates in the transition region lie below the HRG estimates even after corrections accounting for the distorted pion spectrum have been applied. Thus, our conclusion is that at the highest RHIC energies and at the LHC, the width of probability distribution for the net electric charge should be narrower than what HRG model calculations would suggest since $\hat{\chi}_2^Q$ in Eq. 15 is smaller.

In the case of the net baryon number fluctuations, deviations from HRG model results start to become statistically significant only for $T \gtrsim 165$ MeV and will therefore be hard to quantify. We also find that the ratio of the net baryon number and electric charge fluctuations, presented in Fig. 6, approaches the HRG model result from above and starts to agree with it for $T \lesssim 150$ MeV. In the transition region this ratio is

$$\frac{\chi_2^B}{\chi_2^Q} \simeq (0.29 - 0.35) \quad \text{for} \quad 160 \text{ MeV} \le T \le 170 \text{ MeV} \ , \tag{16}$$

i.e., fluctuations in net electric charge are expected to be about three to four times larger in the vicinity of the freeze-out temperature in heavy ion collisions than net baryon number fluctuations. It is worth noting that a comparison of χ_2^B/χ_2^Q with the ratio of proton to net charge fluctuations, which is accessible in heavy ion collisions, will allow us to relate fluctuations in the proton number to the fluctuations of the conserved net baryon number [38].

Finally, we point out that the continuum extrapolated results presented here, and summarized in Table VI in a temperature regime relevant to the freeze-out conditions in heavy ion collisions, do not rely on any uncertainties in the determination of the QCD crossover temperature or its characterization through different observables as discussed in [27]. Systematic errors on the temperature values listed in the first row of Table VI can only come from uncertainties in the zero-temperature observable used to determine the temperature scale. We estimate these uncertainties to be less than 2 MeV in our calculation [27].

APPENDIX: CHOICE OF TEMPERATURE SCALE AND THE HADRON SPECTRUM

In this appendix we discuss the effect of setting the scale using different observables with mass-dimension one calculated in zero-temperature simulations. We denote lattice observables measured in units of the lattice spacing and calculated at a given β by $O_i(\beta)$. In the limit $\beta \equiv 10/g^2 \to \infty$, these approach their physical value O_i^{phy} as

$$O_i(\beta) = \frac{O_i^{phy}}{\Lambda_L} R(\beta) \left(1 + g^2 b_i R^2(\beta) \right) \ . \tag{17}$$

where Λ_L is the QCD scale, $R(\beta) \equiv a(\beta)\Lambda_L$ is the β-function, and only the leading correction $\mathcal{O}(g^2 a^2)$, relevant to our tree-level improved staggered formulation, has been retained.

Consider using the observable O_i to define the temperature scale T_i. On a lattice of temporal size N_τ, this temperature is given in terms of O_i^{phy} as

$$T_i(\beta) = \frac{O_i^{phy}}{O_i(\beta)N_\tau} \tag{18}$$

The ratio of any two such temperature scales is then given by

$$\begin{aligned}
\frac{T_1(\beta)}{T_2(\beta)} &= \frac{O_1^{phy}}{O_1(\beta)} \frac{O_2(\beta)}{O_2^{phy}} \\
&= \frac{1 + b_2 g^2 R^2(\beta)}{1 + b_1 g^2 R^2(\beta)} \\
&\approx 1 + (b_2 - b_1)g^2 R^2(\beta) \ .
\end{aligned} \tag{19}$$

Using Eqs. (18) and (19) we can express the observable $O_2(\beta)$ in terms of the temperature scale T_1 obtained from O_1 as

$$O_2(\beta)N_\tau = \frac{O_2^{phy}}{T_2} \approx \frac{O_2^{phy}}{T_1}\left(1 + (b_2 - b_1)g^2 R^2(\beta)\right) \ . \tag{20}$$

This shows that if an observable of interest (O_2) has a cut-off dependence similar to that of observable (O_1) used to determine the temperature scale T_1, i.e., $b_2 \simeq b_1$, then $O_2(\beta)N_\tau$, as an estimate of O_2^{phy}/T_1, has small cutoff effects. Since all the $b_i - b_1$ need not be small, improving the scaling behavior of one observable does not, in general, imply improvement in all observables.

In the low temperature regime of QCD, the relevant degrees of freedom are hadrons with masses M_H. If the hadron resonance gas is a good approximation in this regime, continuum extrapolations of lattice data are better controlled if a temperature scale is chosen such that all the lattice estimates of M_H/T have small cut-off dependences. We find that using a hadronic observable such as f_K improves the scaling behavior of the susceptibilities and correlations between charges as shown in Fig. 4.

The pion sector is, however, different and has enhanced cut-off effects due to taste symmetry breaking. One does not, therefore, expect to absorb all these effects with a choice of the temperature scale. For this reason we had to modify the HRG analysis to compare with lattice data for charge fluctuations which are dominated by contributions from the pions.

---

[1] H. Caines [STAR Collaboration], [arXiv:0906.0305 [nucl-ex]];
    G. Odyniec [STAR Collaboration], J. Phys. G **35**, 104164 (2008).
[2] M. M. Aggarwal *et al.* [STAR Collaboration], Phys. Rev. Lett. **105**, 022302 (2010).
[3] M. Asakawa and K. Yazaki, Nucl. Phys. A **504**, 668 (1989).
[4] J. Berges and K. Rajagopal, Nucl. Phys. B **538**, 215 (1999);
    A. M. Halasz, A. D. Jackson, R. E. Shrock, M. A. Stephanov, and J. J. M. Verbaarschot, Phys. Rev. D **58**, 096007 (1998).
[5] F. Karsch, arXiv:1202.4173 [hep-lat], presented at the International Conference "Critical Point and Onset of Deconfinement - CPOD 2011", Wuhan, November 7-11, 2011.
[6] F. Karsch and K. Redlich, Phys. Lett. B **695**, 136 (2011).
[7] B. Friman, F. Karsch, K. Redlich, and V. Skokov, Eur. Phys. J. C **71**, 1694 (2011), [arXiv:1103.3511 [hep-ph]].
[8] P. Braun-Munzinger, B. Friman, F. Karsch, K. Redlich, and V. Skokov, [arXiv:1107.4267 [hep-ph]].
[9] P. Braun-Munzinger, K. Redlich, and J. Stachel, In *Hwa, R.C. (ed.) et al.: Quark gluon plasma* 491-599, [nucl-th/0304013].
[10] A. Andronic, P. Braun-Munzinger, J. Stachel, and M. Winn, [arXiv:1201.0693 [nucl-th]].
[11] A. Andronic, P. Braun-Munzinger, and J. Stachel, Phys. Lett. B **673**, 142 (2009), [Erratum-ibid. B **678**, 516 (2009)] [arXiv:0812.1186 [nucl-th]].
[12] R. Dashen, S.-K. Ma and H.J. Bernstein, Phys. Rev. 187, 345 (1969).
[13] R. Venugopalan and M. Prakash, Nucl. Phys. A **546**, 718 (1992).
[14] F. Becattini, J. Phys.: Conf. Ser. 5, 175 (2005).
[15] J. Cleymans, H. Oeschler, K. Redlich and S. Wheaton, Phys. Rev. C **73**, 034905 (2006).
[16] S. Ejiri, F. Karsch, and K. Redlich, Phys. Lett. B **633**, 275 (2006).
[17] S. A. Gottlieb, W. Liu, D. Toussaint, R. L. Renken, and R. L. Sugar, Phys. Rev. Lett. **59**, 2247 (1987).

[18] R. V. Gavai, S. Gupta, and P. Majumdar, Phys. Rev. D **65**, 054506 (2002), [hep-lat/0110032].

[19] C. Bernard *et al.* [MILC Collaboration], Phys. Rev. D **71**, 034504 (2005). [hep-lat/0405029].

[20] M. Cheng, P. Hegde, C. Jung, F. Karsch, O. Kaczmarek, E. Laermann, R. D. Mawhinney, C. Miao, P. Petreczky, C. Schmidt, and W. Soeldner, Phys. Rev. D **79**, 074505 (2009).

[21] S. Borsanyi, Z. Fodor, S. D. Katz, S. Krieg, C. Ratti, and K. Szabo, [arXiv:1112.4416 [hep-lat]].

[22] V. Koch, A. Majumder, and J. Randrup, Phys. Rev. Lett. **95**, 182301 (2005).

[23] C. R. Allton, M. Doring, S. Ejiri, S. J. Hands, O. Kaczmarek, F. Karsch, E. Laermann, and K. Redlich, Phys. Rev. D **71**, 054508 (2005), [hep-lat/0501030].

[24] S. Mukherjee, J. Phys. G G **38**, 124022 (2011), [arXiv:1107.0765 [nucl-th]].

[25] P. Hegde (for the HotQCD Collaboration), arXiv:1110.5932 [hep-lat].

[26] E. Follana *et al.* [HPQCD collaboration and UKQCD collaboration], Phys. Rev. D **75** 054502 (2007), [arXiv:hep-lat/0610092].

[27] A. Bazavov *et al.* [HotQCD Collaboration], arXiv:1111.1710 [hep-lat].

[28] K. Nakamura *et al.* (Particle Data Group), J. Phys. G **37**, 075021 (2010).

[29] See for instance: J. Kapusta and C. Gale, *Finite Temperature Field Theory*, Cambridge University Press, 2006.

[30] A. Bazavov, *et al.* [MILC Collaboration], PoS **LATTICE2010**, 074 (2010), [arXiv:1012.0868 [hep-lat]].

[31] Y. Aoki, S. Borsanyi, S. Durr, Z. Fodor, S. D. Katz, S. Krieg, and K. K. Szabo, JHEP **0906**, 088 (2009).

[32] F. Karsch, K. Redlich, and A. Tawfik, Phys. Lett. B **571**, 67 (2003).

[33] U. M. Heller, F. Karsch, and B. Sturm, Phys. Rev. D **60**, 114502 (1999), [hep-lat/9901010].

[34] P. Huovinen and P. Petreczky, Nucl. Phys. A **837**, 26 (2010).

[35] S. Jeon and V. Koch, Phys. Rev. Lett. **85**, 2076 (2000).

[36] A. Majumder and B. Muller, Phys. Rev. C **74**, 054901 (2006), [nucl-th/0605079].

[37] J.-P. Blaizot, E. Iancu, and A. Rebhan, Phys. Lett. B **523**, 143 (2001).

[38] M. Kitazawa and M. Asakawa, Phys. Rev. C **85**, 021901 (2012), [arXiv:1107.2755 [nucl-th]].